Recombination activity of interstitial chromium and chromium-boron pairs in silicon

Jan Schmidt,[a] Rafael Krain, and Karsten Bothe
Institut für Solarenergieforschung Hameln/Emmerthal (ISFH), Am Ohrberg 1, D-31860 Emmerthal, Germany

Gerhard Pensl and Svetlana Beljakowa
Lehrstuhl für Angewandte Physik (LAP), Universität Erlangen-Nürnberg, Staudtstraße 7, D-91058 Erlangen, Germany

(Received 25 June 2007; accepted 22 October 2007; published online 17 December 2007)

The recombination activity of interstitial chromium (Cr_i) and pairs of interstitial chromium and substitutional boron (Cr_iB_s) in crystalline silicon is studied by combining temperature- and injection-dependent lifetime and deep-level transient spectroscopy measurements on intentionally chromium-contaminated *n*- and *p*-type silicon wafers. Cr_i as well as Cr_iB_s pairs are found to be one order of magnitude less recombination active than widely assumed. In the case of Cr_i, a defect energy level of $E_C-E_t=0.24$ eV, an electron capture cross section of $\sigma_n=2\times10^{-14}$ cm^2, and a hole capture cross section of $\sigma_p=4\times10^{-15}$ cm^2 are determined. For Cr_iB_s pairs, measurements on boron-doped *p*-type silicon result in $E_t-E_V=0.28$ eV, $\sigma_n=5\times10^{-15}$ cm^2, and $\sigma_p=1\times10^{-14}$ cm^2. Theoretical calculations using the Shockley–Read–Hall theory show that it depends crucially on the doping concentration whether Cr_i or Cr_iB_s is the more active recombination center. Using a calibration function calculated from the defect parameters determined in this study, lifetime changes measured before and after thermal dissociation of Cr_iB_s pairs can be used to determine the interstitial chromium concentration in boron-doped silicon. © *2007 American Institute of Physics*. [DOI: 10.1063/1.2822452]

I. INTRODUCTION

Chromium is detrimental to silicon-based devices, as it strongly reduces the recombination lifetime of crystalline silicon.[1] In particular in photovoltaics, relatively high concentrations of chromium have been measured in multicrystalline silicon wafers, used today in the majority of commercially produced solar cells. Using neutron activation analysis (NAA) Macdonald *et al.* determined the total chromium concentration of different block-cast multicrystalline silicon wafers to be in the range of $1-2\times10^{13}$ cm^{-3}.[2,3] Istratov *et al.*[4] even detected chromium concentrations of up to 1.8×10^{15} cm^{-3} by NAA in multicrystalline silicon wafers grown by sheet technology. Despite the relatively high chromium contents measured in multicrystalline silicon materials, the actual state of most of the chromium is still a matter of discussion. Recent investigations by Buonassisi *et al.*[5] using synchrotron-based analytical x-ray microprobe techniques suggest that generally most metals in multicrystalline silicon are present in the form of nanoprecipitates or metal-rich inclusions. As these metal-rich particles can be relatively large (up to tens of microns), their density and therefore their recombination activity is typically well below that of the isolated metal atoms. Hence, the carrier lifetime of chromium-contaminated silicon is mainly related to recombination via isolated interstitial chromium atoms (Cr_i) and, in the case of boron-doped silicon, via defect pairs of interstitial chromium and substitutional boron (Cr_iB_s pairs).[6–11] Unfortunately, relatively little is known about the recombination activity of Cr_i and Cr_iB_s pairs in silicon at room temperature, that is, only very few data have been published until now concerning the electron and hole capture cross sections of these recombination centers at room temperature.[9,10] An accurate knowledge of these defect parameters would be highly valuable for the determination of the interstitial chromium content from lifetime measurements and also for predicting the impact of chromium contamination on device performance.

This paper aims at gaining an improved knowledge of the recombination parameters of Cr_i and Cr_iB_s pairs in crystalline silicon at temperatures corresponding to typical device operating conditions. We extract the concentrations of Cr_i and Cr_iB_s pairs in deliberately chromium-contaminated, boron-, and phosphorus-doped *p*- and *n*-type silicon wafers by means of deep-level transient spectroscopy (DLTS). On the same samples, temperature- and injection-dependent lifetime spectroscopy (TIDLS) measurements are performed. The measured TIDLS data are fitted using the Shockley–Read–Hall (SRH) theory, from which energy levels and capture cross sections are determined. Using the experimentally determined defect parameters, we calculate calibration factors for the determination of the interstitial chromium concentration in boron-doped silicon by measuring the lifetimes before and after thermal Cr_iB_s dissociation. This results in a highly sensitive quantitative chromium detection method based on easy-to-use contactless lifetime measurements.

II. CR_i AND CR_iB_s PAIRS IN SILICON

All interstitial 3*d* transition metals form donor levels in silicon so that they are positively charged in *p*-type silicon.[8]

[a]Electronic mail: j.schmidt@isfh.de.

Due to the fact that interstitial transition metals are highly mobile in the silicon lattice, the mobile positive metal ions can be captured by negatively charged substitutional acceptors, forming donor-acceptor pairs. One of the most frequently studied examples of such a defect pair in silicon is the prominent Fe_iB_s pair, however, the same type of defect reaction is also observed for the less studied Cr_iB_s pair.[8,11] It has been shown that the donor-acceptor pair formation indeed only occurs if Coulomb attraction is present. If the Fermi level is shifted above the energy level of the donor state, e.g., by overcompensating boron-doped silicon with phosphorus, the metal impurity is in its neutral charge state and no pair formation is observed.[8]

First evidence of a donor level correlated with interstitial chromium in silicon was provided by Woodbury and Ludwig[6] using electron paramagnetic resonance (EPR) measurements. These measurements were later confirmed by DLTS (Refs. 12 and 13) as well as Hall effect measurements.[14] Today, an energy level of $E_C-E_t=0.22\pm0.02$ eV is well established for the donor state of Cr_i in silicon.[11] This energy level is relatively close to the conduction band edge E_C and, hence, Cr_i is present in its positive charge state in *p*-type silicon as well as in *n*-type silicon if the doping concentration is below $N_{dop}=4\times10^{15}$ cm^{-3}, corresponding to a Fermi level below the Cr_i level at room temperature. Unlike Fe_i surprisingly little is known concerning the recombination activity of Cr_i in silicon. The few published data for the electron capture cross section σ_n strongly scatter between 3×10^{-15} cm^2 and 2×10^{-13} cm^2.[15,9] A comprehensive survey of DLTS literature data by Graff resulted in an average value of $\sigma_n=7.3\times10^{-15}$ cm^2 at ~110 K.[11] For the hole capture cross section σ_p of Cr_i in silicon only a single, very large value of 1×10^{-13} cm^2 extracted from carrier lifetime measurements at room temperature has been published so far.[9] In the same study, a very high room-temperature electron capture cross section of $\sigma_n=2\times10^{-13}$ cm^2 has been determined.

Cr_iB_s pairs produce a single donor level in the lower half of the silicon band gap, as has been determined by DLTS (Ref. 12) and confirmed by combination of DLTS, EPR, and photoluminescence measurements.[13] Most measurements agree well in that the energy level of the Cr_iB_s pair is located at $E_t-E_V=0.28\pm0.02$ eV.[11] Less consistent, however, is the experimental data published on the capture cross sections. Hole capture cross sections σ_p measured by DLTS at ~150 K range from 10^{-15} to 10^{-14} cm^2,[11,13] whereas the electron capture cross section σ_n was estimated by Conzelmann *et al.*[13] to be about 2×10^{-13} cm^2. Only few studies reporting capture cross sections of Cr_iB_s pairs in silicon at room temperature, all based on carrier lifetime measurements, have been published until now. Mishra[9] determined a room-temperature electron capture cross section of $\sigma_n=1\times10^{-13}$ cm^2, whereas Hangleiter[16] published $\sigma_n=5\times10^{-14}$ cm^2 and $\sigma_p=2\times10^{-14}$ cm^2 at 300 K. More recently, Dubois *et al.*[17] published a hole capture cross section of $\sigma_p=8\times10^{-14}$ cm^2.

III. EXPERIMENTAL DETAILS

A. Sample preparation

The samples studied in this paper are phosphorus- and boron-doped (100)-oriented Czochralski-grown silicon (Cz-Si) wafers of 620 μm thickness. Chromium was added directly to the silicon melt during crystal growth. Total chromium concentrations of 1.7 and 1.6×10^{13} cm^{-3} were measured by NAA in the *n*- and the *p*-type material, respectively.[18] The wafers are polished on one side and lapped on the other. The interstitial oxygen content of all Cz-Si wafers used in this study, as determined by infrared absorption, is in the range of $(7-8)\times10^{17}$ cm^{-3}, whereas the substitutional carbon content is below the detection limit of 5×10^{15} cm^{-3}. Using four-point-probe measurements, we determine the resistivities of the wafers to be 2.7 Ω cm for the *n*-Si and 11.4 Ω cm for the *p*-Si material. These resistivities correspond to a donor concentration of $N_D=1.7\times10^{15}$ cm^{-3} in the *n*-Si and an acceptor concentration of $N_A=1.2\times10^{15}$ cm^{-3} in the *p*-Si wafers. Due to the relatively low boron concentration in the *p*-Si material, the effect of boron-oxygen-related recombination centers on the lifetime can be neglected.[19]

For the TIDLS measurements, the wafers are RCA cleaned and both sides are passivated by means of remote plasma-enhanced-chemical-vapor-deposited silicon nitride films. This passivation scheme provides very low surface recombination velocities <10 cm/s on silicon surfaces,[20,21] which was verified on noncontaminated control wafers of the same type. Hence, surface recombination can be completely neglected for all lifetime samples investigated in this study. The relatively low silicon nitride deposition temperature of 400 °C for a few minutes avoids potential precipitation problems that might occur if high-temperature processes, such as oxidation, had been applied for surface passivation.

For the DLTS measurements, circular Schottky contacts with diameters ranging from 0.2 to 1 mm are deposited onto the polished front side of the wafers. Gold is thermally evaporated to form the Schottky contact on the *n*-Si material and a stack of titanium and aluminum is sputtered onto the *p*-type silicon. In both cases, the Ohmic contact is formed on the lapped rear side of the wafers by sputtering of aluminum.

B. TIDLS

The contactless quasi-steady-state photoconductance (QSSPC) method developed by Sinton and Cuevas[22] is used to measure the lifetime as a function of injection level. In order to enable temperature-dependent measurements, the original QSSPC setup (Sinton Consulting, Inc.) has been complemented with a temperature-controlled sample stage positioned on top of the photoconductance-sensor coil.[23,24] The sample is placed on a Pyrex glass disk kept in a distance of about 1 mm from the coil by means of insulating spacers. The edge of the wafer is brought in contact with a brass ring, which is heated using a resistive element. The temperature of the sample is measured with a thermocouple mounted on its surface and the heating power is regulated via a proportional controller. This setup allows TIDLS measurements in the temperature range between 30 and 170 °C. For the determi-

nation of the carrier lifetime from the measured photoconductance data, it is very important to take the temperature dependence of the mobility into account. In this work, this was done using the empirical mobility parameterization of Arora *et al.*[25] The small changes in the generation rate G can be neglected in the investigated temperature range (rising the temperature from 30 to 170 °C leads to an increase in G of only 5%). The total lifetime measurement error is estimated to be about 10%.

We evaluate the TIDLS measurements by fitting the SRH equation simultaneously to the measured set of injection-dependent lifetime curves recorded at different temperatures. Provided the density of recombination centers N_t is sufficiently small,[26] the recombination lifetime can be modeled by traditional SRH statistics.[27,28] For interstitial chromium in silicon this prerequisite is virtually always valid because of its relatively low solubility in silicon.[11] Assuming negligible trapping and, hence, equal excess electron and hole concentrations ($\Delta n = \Delta p$), the SRH lifetime τ_{SRH} associated with a single-level defect in silicon of equilibrium electron and holes concentrations n_0 and p_0, respectively, is given by[29]

$$\tau_{\mathrm{SRH}}(\Delta n, T) = \frac{\tau_{n0}(p_0 + p_1 + \Delta n) + \tau_{p0}(n_0 + n_1 + \Delta n)}{p_0 + n_0 + \Delta n}, \quad (1)$$

where the electron and hole capture time constants τ_{n0} and τ_{p0} are related to the defect density N_t, the thermal velocity v_{th}, and the electron and hole capture cross sections σ_n and σ_p via $\tau_{n0} = (\sigma_n v_{\mathrm{th}} N_t)^{-1}$ and $\tau_{p0} = (\sigma_p v_{\mathrm{th}} N_t)^{-1}$. The temperature dependence of the capture time constants is mainly due to the temperature dependence of the thermal velocity given by the expression

$$v_{\mathrm{th}}(T) = v_{\mathrm{th}}^{300\ \mathrm{K}} \left(\frac{T}{300\ \mathrm{K}} \right)^{1/2}, \quad (2)$$

where $v_{\mathrm{th}}^{300\ \mathrm{K}} = 1.1 \times 10^7$ cm/s is the thermal velocity of the carriers at $T = 300$ K.[30] An additional temperature dependence of τ_{n0} and τ_{p0} may arise from temperature-dependent capture cross sections. As a first approximation we assume σ_n and σ_p to be temperature independent and define $k \equiv \sigma_n / \sigma_p = \tau_{p0} / \tau_{n0}$ as symmetry factor characteristic of the specific defect under investigation. In case a complete fit of all measured temperature- and injection-dependent lifetime curves is not possible using a single set of defect parameters, we adjust the temperature dependences of σ_n and σ_p.

The densities n_1 and p_1 in Eq. (1) equal the equilibrium electron and hole densities when the defect energy level E_t coincides with the Fermi level

$$n_1(E_t, T) = N_C(T) \exp\left(-\frac{E_C - E_t}{kT} \right),$$
$$p_1(E_t, T) = N_V(T) \exp\left(-\frac{E_t - E_V}{kT} \right). \quad (3)$$

The temperature dependence of the effective density of states in the conduction band $N_C(T)$ and in the valence band $N_V(T)$ is to a good approximation given by

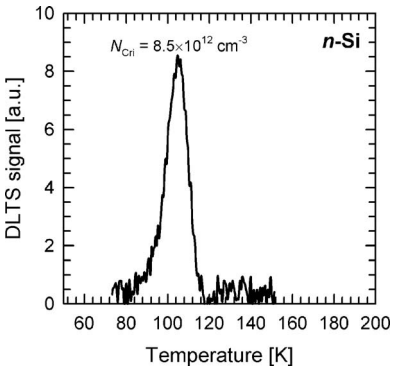

FIG. 1. DLTS spectrum measured on an intentionally Cr-contaminated n-type silicon wafer. The Arrhenius plot of the peak temperature gives an energy level of $E_C - E_t = 0.22$ eV, which can be assigned to the Cr_i donor level in silicon, and an electron capture cross section of $\sigma_n = (2.1 \pm 1.0) \times 10^{-14}$ cm^2.

$$N_C(T) = N_C^{300\ \mathrm{K}} \left(\frac{T}{300\ \mathrm{K}} \right)^{3/2},$$
$$N_V(T) = N_V^{300\ \mathrm{K}} \left(\frac{T}{300\ \mathrm{K}} \right)^{3/2}, \quad (4)$$

where the effective densities of states at 300 K are taken as $N_C^{300\ \mathrm{K}} = 2.86 \times 10^{19}$ cm^{-3} and $N_V^{300\ \mathrm{K}} = 3.10 \times 10^{19}$ cm^{-3}.[31] Note that in this study we only account for SRH recombination and neglect all other recombination channels, such as Auger and radiative recombination.

C. DLTS

Defect concentrations and energy levels are measured by means of a digital Fourier-transform deep-level transient spectroscopy system (PhysTech) using a 1 MHz Boonton bridge in combination with a fast pulse generator.[32,33] A filling pulse length of 1 ms is applied in all the standard DLTS measurements performed in this study. The correlation function used for the representation of the DLTS spectra corresponds to the normalized first Fourier sine coefficient in a predefined time window. The defect energy level is obtained from an Arrhenius plot of the peak temperature measured at different time windows and the defect concentration from the corresponding peak height.

IV. RESULTS AND DISCUSSION

A. Interstitial chromium

Figure 1 shows a DLTS spectrum measured on the intentionally chromium-contaminated n-type silicon sample. The DLTS peak observed in the n-type material can be assigned to interstitial chromium. The Arrhenius analysis results in an energy level of $E_C - E_t = 0.22$ eV, which is in excellent agreement with DLTS literature data for the donor state of Cr_i in silicon,[11] and an electron capture cross section σ_n of $(2.1 \pm 1.0) \times 10^{-14}$ cm^2. Note that in this case, the capture cross section includes the entropy factor. We determine the concentration of interstitial chromium in the n-type silicon sample from the height of the DLTS peak to be $N_{\mathrm{Cr}_i} = 8.5 \times 10^{12}$ cm^{-3}. This value is 50% below the total chro-

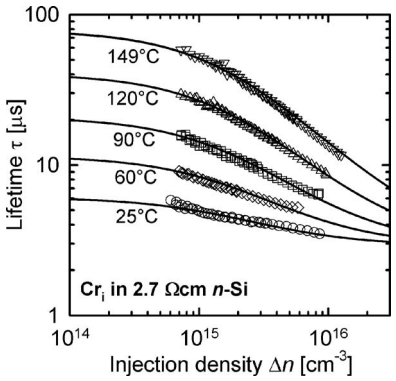

FIG. 2. Injection-dependent lifetime curves measured in the temperature range from 25 to 149 °C (symbols) on the same *n*-type silicon material as measured by DLTS, with Cr_i identified as the most recombination-active impurity. The solid lines show a simultaneous SRH fit to the measured TIDLS data. The detailed DPSS analysis shown in Fig. 3 results in a defect energy level of $E_C-E_t=0.24$ eV, a hole capture time constant of $\tau_{p0}^{300\ \mathrm{K}}=3\ \mu$s, and a symmetry factor of $k=5$.

mium concentration of 1.7×10^{13} cm^{-3} measured by NAA, suggesting that approximately half of the chromium has formed precipitates during the relatively slow cooling process after crystal growth. The chromium precipitates show a strongly reduced recombination activity compared to interstitial chromium, as has been shown in the literature.[4] Hence, we assume that the lifetime in our *n*-type silicon material is limited by isolated Cr_i.

Figure 2 shows injection-dependent lifetime curves in the temperature range from 25 to 149 °C (symbols) measured on the same *n*-type material as has been analyzed by means of DLTS. The solid lines show a simultaneous fit of Eq. (1) to the measured TIDLS data. The entire set of lifetime curves can be well fitted by the SRH model assuming that only one single-level defect determines the lifetime. In order to pin down the true defect parameters, we apply the defect parameter solution surface (DPSS) method proposed by Rein *et al.*[34,35] The fit routine used is based on the Marquardt–Levenberg algorithm and the three fit parameters to be determined are the defect energy level E_t, the hole capture time constant τ_{p0}, and the symmetry factor $k=\tau_{p0}/\tau_{n0}=\sigma_n/\sigma_p$. Figure 3 visualizes the DPSS analysis of the TIDLS curves shown in Fig. 2, where the temperature dependence of τ_{p0} due to the temperature dependence of the thermal velocity v_{th} given by Eq. (2) is removed by multiplying τ_{p0} by $(T/300\ \mathrm{K})^{1/2}$, resulting in the τ_{p0} value at 300 K, $\tau_{p0}^{300\ \mathrm{K}}$, where the hole capture cross section σ_p is assumed to be independent of temperature. For each injection-dependent lifetime curve recorded at a specific temperature, the defect energy level E_t is gradually varied throughout the silicon band gap and optimal fit parameters τ_{p0} and k are determined at each E_t. As can be seen from Figs. 3(a) and 3(b), at a single temperature the injection-dependent lifetime can be well modeled by a broad range of different defect parameters. This ambiguity can be overcome by performing the same type of analysis on lifetime curves measured at different temperatures and plotting the corresponding optimal τ_{p0} and k fit results as a function of E_t in the same plot for the various temperatures, which has been done in Figs. 3(a) and 3(b). Figure 3(b) suggests that there exists an optimal τ_{p0} value valid for all temperatures. In order to determine the τ_{p0} fit parameter with the highest quality, the τ_{p0} values determined at each energy level E_t are averaged and the standard deviation in τ_{p0} is determined. The corresponding plot of the relative standard deviation in τ_{p0} as a function of the energy level E_t is shown in Fig. 3(c). The plot shows that there are two minima, one in the upper, the other in the lower half of the silicon band gap. As the minimal standard deviation in the upper band gap half is well below that in the lower half of the band gap, we identify the solution in the upper band gap half as the most likely defect parameters: $E_C-E_t=0.24\pm0.02$ eV and $\tau_{p0}^{300\ \mathrm{K}}=3\pm1\ \mu$s. Using the Cr_i concentration of $N_{\mathrm{Cr}_i}=8.5\times10^{12}$ cm^{-3} measured by DLTS on the same material, a hole capture cross section of $\sigma_p=(4\pm1)\times10^{-15}$ cm^2 is obtained. The result that σ_p is temperature independent suggests a multiphonon capture process for holes. In the case of the cascade capture process, the capture cross section would be expected to vary with T^{-1} to

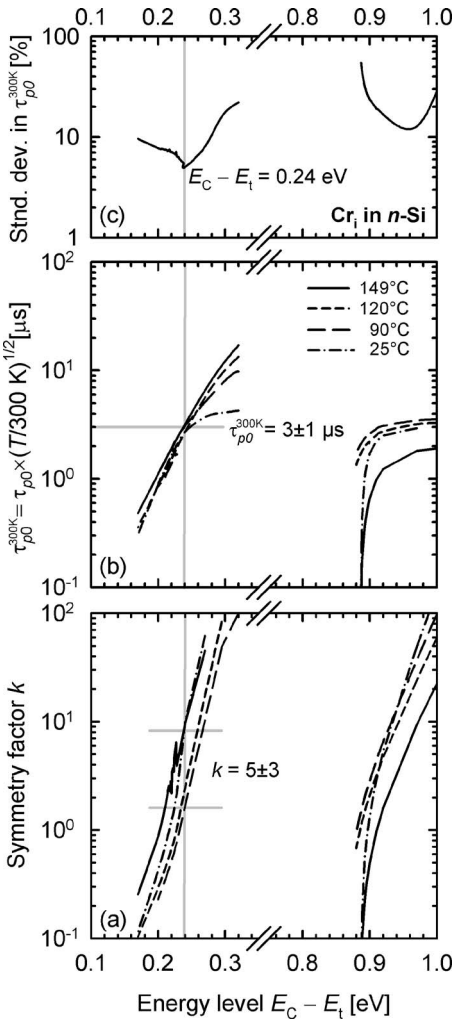

FIG. 3. DPSS analysis of the TIDLS curves shown in Fig. 2. For each injection-dependent lifetime curve recorded at a specific temperature, the defect energy level E_t is gradually varied throughout the silicon band gap and best fit parameters for (a) the symmetry factor k and (b) the hole capture time constant τ_{p0} are determined at each value of E_t. The temperature dependence of τ_{p0} due to the temperature dependence of the thermal velocity is removed by multiplying τ_{p0} by $(T/300\ \mathrm{K})^{1/2}$, resulting in $\tau_{p0}^{300\ \mathrm{K}}$. (c) Relative standard deviation in $\tau_{p0}^{300\ \mathrm{K}}$, showing that the optimal solution is obtained for $E_C-E_t=0.24\pm0.02$ eV, $\tau_{p0}^{300\ \mathrm{K}}=3\pm1\ \mu$s, and $k=5\pm3$.

T^{-3}, depending on the defect potential. For strong lattice coupling multiphonon capture dominates, which may result in two different temperature dependences.[36] For phonon energies $\hbar\omega \ll kT$ a thermally activated temperature dependence of the capture cross section is expected, whereas for $\hbar\omega > kT$ theory predicts a temperature-independent capture cross section.[36] As for optical phonons in silicon $\hbar\omega \approx 60$ meV and the maximum temperature applied in this study of 149 °C corresponds to $kT=36.5$ meV, a multiphonon capture process would lead to a temperature-independent capture cross section.

The determination of the symmetry factor k from Fig. 3(a) turns out to be more difficult compared to the E_t and τ_{p0} determination. This is mainly due to fact that the fit curves are relatively insensitive to variations in k, resulting in a broad scatter in the set of possible k fit parameters at each energy level. As the true defect energy level has already been pinned down to $E_C - E_t = 0.24$ eV, the set of k fit parameters determined at this particular energy level results in $k = \sigma_n/\sigma_p = 5 \pm 3$, as can be seen from Fig. 3(a). Using the σ_p value determined in the earlier analysis, an electron capture cross section of $\sigma_n = (2 \pm 1) \times 10^{-14}$ cm^2 is obtained. A possible temperature dependence of σ_n is difficult to extract from our TIDLS measurements alone, as the uncertainty in the determined k values is too large to reveal small temperature dependences. However, the excellent agreement with the electron capture cross section determined from our DLTS measurements at ~110 K suggests that σ_n of Cr_i in Si is in fact not temperature dependent in the broad temperature range between ~100 and 400 K. The energy level of $E_C - E_t = 0.24 \pm 0.02$ eV determined by TIDLS is in good agreement with the widely accepted DLTS energy level of $E_C - E_t = 0.22 \pm 0.02$ eV for Cr_i in Si.[11] Hence, we can identify the recombination center limiting the carrier lifetime in our n-type sample with interstitial chromium. The electron capture cross section of $\sigma_n = (2 \pm 1) \times 10^{-14}$ cm^2 is also in good agreement with DLTS data published by Nakashima *et al.*,[38] who reported $\sigma_n = 1.4 \times 10^{-14}$ cm^2 (at 110 K). On the other hand, the capture cross sections determined in our analysis are approximately one order of magnitude below the huge capture cross sections $> 10^{-13}$ cm^2 determined in the lifetime study by Mishra,[9] although the capture cross section ratio of $k=2$ determined in the same study agrees well with our result of $k = 5 \pm 3$. The positive charge state of Cr_i can be made responsible for the observed asymmetry in the capture cross sections.

B. Chromium-boron pairs

Figure 4 shows injection-dependent lifetime curves of the chromium-contaminated boron-doped p-type silicon material measured as a function of time after annealing the sample for 30 min at 250 °C. This anneal completely dissociates all chromium-boron pairs.[13] Between each lifetime measurement the sample is stored at 69 °C, while the lifetime measurements are all performed at room temperature. As seen from Fig. 4, the lifetime of the sample decreases with time, which we attribute to the formation of Cr_iB_s pairs. After approximately 30 h of annealing at 69 °C the lifetime saturates. The experiment was continued for additional 70 h without observing any further changes in lifetime. From an exponential fit to the time-dependent lifetime data at a fixed injection level, we determine the chromium-boron association time constant at 69 °C to be $\tau_{assoc} = 10$ h. In order to compare this time constant with literature data, we assume that the pair formation reaction is governed by the diffusion of the positively charged Cr_i^+ to the negatively charged immobile B_s^-. Assuming Coulomb attraction between the pairing species, the association time constant τ_{assoc} in units of seconds is given by the expression[37]

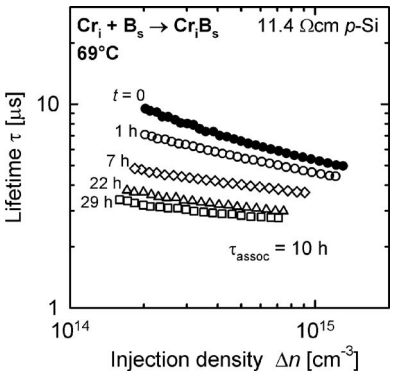

FIG. 4. Injection-dependent lifetime curves measured on Cr-contaminated B-doped p-Si as a function of time after complete dissociation of all Cr_iB_s pairs into interstitial Cr_i and substitutional B_s by annealing the sample for 30 min at 250 °C. Between each lifetime measurement, carried out at room temperature, the sample is stored at 69 °C. After approximately 30 h of annealing the lifetime saturates, indicating complete repairing. From an exponential fit to the time-dependent lifetime data, the Cr_iB_s association time constant is determined to $\tau_{assoc} = 10$ h.

$$\tau_{assoc} = 557 \frac{T}{N_{dop} D(Cr_i)}, \tag{5}$$

where $D(Cr_i)$ in units of cm^2/s is the diffusivity of interstitial chromium in silicon and N_{dop} in units of cm^{-3} is the boron doping concentration. Nakashima *et al.*[38] have determined the diffusivity of Cr_i in Si at 70 °C to be $D(Cr_i, 70\,°C) = 2 \times 10^{-15}$ cm^2/s. Inserting this value together with the doping concentration of $N_{dop} = 1.2 \times 10^{15}$ cm^{-3} into Eq. (5) gives an association time constant of $\tau_{assoc} = 22$ h. This value is in reasonable agreement with our measured value of 10 h, supporting that the observed lifetime degradation is in fact due to the formation of chromium-boron pairs. Note that the chromium-boron pairing reaction is much slower than the iron-boron pair formation, which at the same temperature of 70 °C would result in an association time constant of only 10 min.[39] This is due to the fact that the diffusivity of Cr_i in Si is approximately two orders of magnitude lower compared to that of Fe_i in Si. In order to enable the complete pair formation of Cr_i with B_s on a reasonable time scale, storing temperatures well above room temperature have to be used. However, at the same time sample temperatures above ~70 °C have to be avoided as the competing dissociation reaction takes place at elevated temperatures. Hence, in our experiments we apply 55 °C for 1 week (association time constant ~55 h) to produce the fully associated state.

Figure 5 shows injection-dependent lifetime measurements recorded on the same sample as in Fig. 4 at different

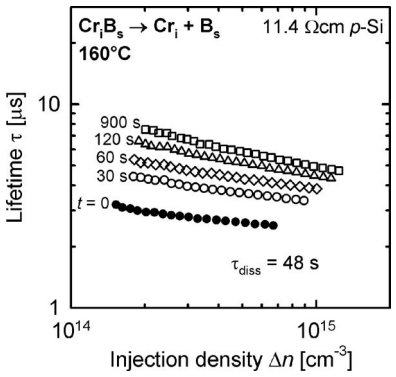

FIG. 5. Injection-dependent lifetime curves measured on the same Cr-contaminated B-doped *p*-Si sample as in Fig. 4 at different times after fully associating the Cr_iB_s pairs by a 1-week anneal at 55 °C. Between each lifetime measurement, carried out at room temperature, the sample is annealed at 160 °C. The observed lifetime increase can be assigned to the thermal dissociation of Cr_iB_s pairs into interstitial Cr_i and substitutional B_s. A dissociation time constant of τ_{diss}=48 s is obtained from an exponential fit to the time-dependent lifetime data.

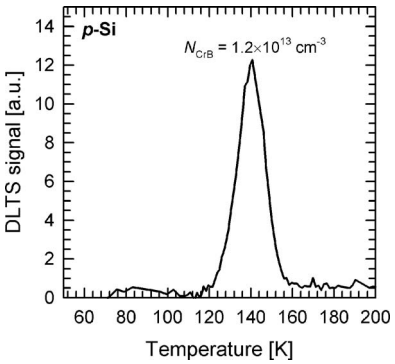

FIG. 6. DLTS spectrum measured on intentionally Cr-contaminated *p*-Si after storage for 1 week at 55 °C. The DLTS peak can be assigned to the donor state of the Cr_iB_s pair. The Arrhenius plot results in an energy level of E_t-E_V=0.28 eV and a hole capture cross section of $\sigma_p=(1.1\pm0.5)\times10^{-14}$ cm^2.

times after fully associating the Cr_iB_s pairs by a 1-week anneal at 55 °C. Between each measurement performed at room temperature the sample is kept at 160 °C in the dark, which reverses the lifetime degradation shown in Fig. 4. The lifetime recovery observed in Fig. 5 can be assigned to the thermal dissociation of Cr_iB_s pairs. A dissociation time constant of τ_{diss}=48 s is deduced from the time-dependent lifetime measurements shown in Fig. 5, making the thermal pair dissociation a relatively fast process.

In the case of Fe_iB_s pairs, it has been found that illumination or injection of minority carriers leads to an effective pair dissociation even at room temperature.[40] This has been attributed to a recombination-enhanced pair dissociation process in combination with a retardation of the repairing reaction. The reason for this retardation is that if the electron quasi-Fermi level rises above the interstitial iron's donor energy level at E_t-E_V=0.38 eV it gets neutralized and the Fe_i will no longer participate in the ion pairing process with B_s^-. This type of electronically stimulated dissociation reaction has not been observed for Cr_iB_s pairs.[9,11] We illuminated the sample in Fig. 4 after complete Cr_iB_s pair formation with a halogen lamp of high intensity (~0.5 W/cm^2) for up to 10 h and were not able to detect any lifetime changes. This result confirms that in fact no electronically stimulated dissociation occurs for Cr_iB_s pairs in silicon.

Figure 6 shows a DLTS spectrum of the *p*-Si sample after storing it for 1 week at 55 °C. The observed DLTS peak can be assigned to the donor state of the Cr_iB_s pair. An energy level of E_t-E_V=0.28 eV and a hole capture cross section of $\sigma_p=(1.1\pm0.5)\times10^{-14}$ cm^2 are obtained from the Arrhenius plot, in excellent agreement with the energy level of the Cr_iB_s pair reported in the literature.[11] The concentration of Cr_iB_s pairs is determined from the DLTS peak height to be $N_{CrB}=1.2\times10^{13}$ cm^{-3}. This concentration is 25% below the total chromium concentration of 1.6×10^{13} cm^{-3} measured on the same material by NAA.

In order to narrow down the uncertainty range of the hole capture cross section of the Cr_iB_s pair, we use the DLTS filling pulse variation technique.[41] This technique is based on measuring the DLTS peak height ΔC_{peak} as a function of the filling pulse length t_p. With increasing length of the filling pulse the height of the DLTS peak increases and eventually saturates when the defect centers under investigation are completely filled with majority carriers. The capture cross section can then be obtained by fitting the equation

$$\Delta C_{peak}(t_p) = \Delta C_{peak}(t_p \rightarrow \infty)[1 - \exp(-\sigma_p p v_{th} t_p)] \qquad (6)$$

to the measured $\Delta C_{peak}(t_p)$ curve. Performing such measurements at different correlation times allows to determine σ_p as a function of temperature within a limited temperature range. Note that the capture cross sections determined by the filling pulse variation technique do not include the entropy factor. In Fig. 7, the symbols show the normalized DLTS peak height $\Delta C_{peak}/\Delta C_{peak}(\infty)$ as a function of the filling pulse length t_p measured for three different correlation times (corresponding to three different temperatures). The hole capture cross-section σ_p is obtained from the least-square fit of Eq. (6) to the experimental data, resulting in $\sigma_p=5.4\times10^{-15}$ cm^2 independent of the temperature (see inset in Fig. 7), indicating that holes are mainly captured via a multiphonon mechanism into the Cr_iB_s pair.

Figure 8 shows injection-dependent lifetime curves recorded at 25 and 70 °C (symbols) on the same chromium-contaminated *p*-Si material as used in the DLTS measure-

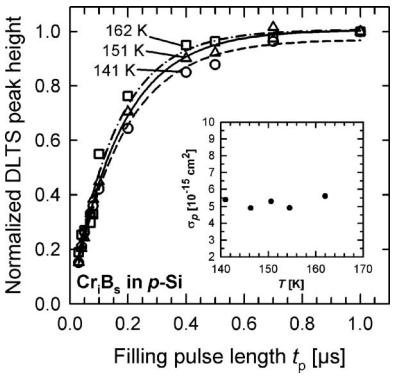

FIG. 7. Normalized DLTS peak height as a function of filling pulse length t_p of Cr_iB_s pairs in *p*-Si measured for different correlation times, corresponding to different temperatures. The temperature dependence of the extracted hole capture cross section σ_p is shown in the inset.

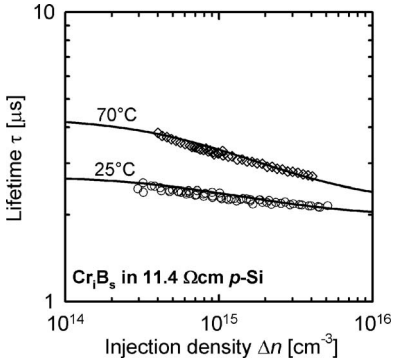

FIG. 8. Injection-dependent lifetime curves measured at 25 and 70 °C (symbols) on Cr-contaminated *p*-Si. Prior to the lifetime measurements the sample was stored for 1 week at 55 °C to ensure that each Cr_i atom is bound to a B_s atom. The temperature range accessible by the lifetime measurements is restricted to temperatures below 70 °C, as higher temperatures dissociate the Cr_iB_s pairs. The solid lines show a SRH fit to the measured lifetime curves using the following defect parameters: $E_t-E_V=0.28$ eV, $\tau_{n0}=1.7$ μs, and $k=0.4$.

ment shown in Fig. 6. Prior to the lifetime measurements the sample was stored for 1 week at 55 °C to ensure that each interstitial chromium atom is bound to substitutional boron. The temperature range accessible by the lifetime measurements is restricted to temperatures below 70 °C, as higher temperatures dissociate the Cr_iB_s pairs. Unfortunately, the narrow limitation of the accessible temperature range results in a very weak temperature dependence of the measured lifetimes. As a consequence of the weak temperature dependence, a complete extraction of all defect parameters from the lifetime data shown in Fig. 8 by the DPSS analysis is not possible for the Cr_iB_s pairs. There exist many different sets of defect parameters, E_t, k, τ_{n0}, resulting in nearly perfect SRH fits to the measured lifetime curves (solid lines in Fig. 8). However, these solutions are highly ambiguous, as seen in Fig. 9, showing the best fit parameters k and τ_{n0} at different assumed defect energy levels E_t for the lifetime curve measured at 25 °C. All fit parameters shown in Fig. 9 result

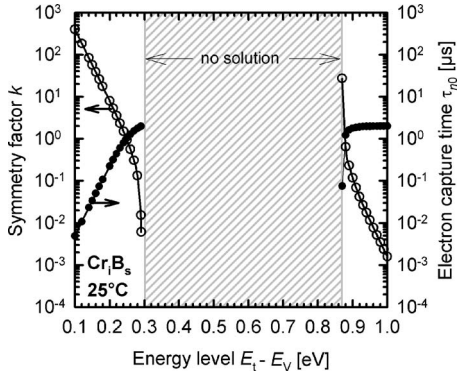

FIG. 9. Best SRH fit parameters k and τ_{n0} at different assumed defect energy levels E_t for the injection-dependent lifetime curve measured at 25 °C (shown in Fig. 6). No satisfactory fit is obtained in the energy range between $E_t-E_V=0.30$ and 0.87 eV. Outside this range various solutions of equally high quality exist. Hence, it is not possible to exactly pin down the Cr_iB_s energy level from this analysis. However, using the energy level of $E_t-E_V=0.28$ eV determined from our DLTS measurements shown in Fig. 1, it is possible to determine the remaining two defect parameters from the lifetime analysis: $\tau_{n0}=1.7\pm0.2$ μs and $k=0.4\pm0.2$.

in fit curves of the same very high quality. The only information which can be extracted from Fig. 9 is that the energy level E_t-E_V of the Cr_iB_s pair must be below 0.3 eV or above 0.87 eV. Hence, it is not possible to extract the exact energy level E_t of the Cr_iB_s pairs from the fit results. However, when we include our DLTS result for the energy level of the Cr_iB_s pair of $E_t-E_V=0.28$ eV it is possible to determine the optimal pair of fit parameters $k=0.4\pm0.2$ and $\tau_{n0}=1.7\pm0.2$ μs from the results displayed in Fig. 9. Using these fit parameters together with the Cr_iB_s concentration of $N_{CrB}=1.2\times10^{13}$ cm^{-3} determined by DLTS we obtain electron and hole capture cross sections of $\sigma_n=(4.5\pm0.5)\times10^{-15}$ cm^2 and $\sigma_p=(1.1\pm0.6)\times10^{-14}$ cm^2, respectively. The fact that the same set of defect parameters can be used to model the injection-dependent lifetime data measured at 25 and 70 °C shown in Fig. 8 suggests that the capture cross sections show only a very weak temperature dependence in the temperature range covered by our lifetime measurements. Importantly, the hole capture cross sections obtained from (i) the DLTS Arrhenius analysis, (ii) the DLTS filling pulse variation method, and (iii) the lifetime spectroscopy analysis agree well within the experimental error ranges of the respective measurement techniques. Since DLTS and lifetime measurements were performed in very different temperature ranges, our results suggest that σ_p is temperature independent over a very broad temperature range between ~140 and 350 K.

The room-temperature electron capture cross section of the Cr_iB_s pair of $\sigma_n=5\times10^{-15}$ cm^2 determined in this work is well below the frequently cited value of $\sigma_n=1\times10^{-13}$ cm^2 published by Mishra,[9] suggesting that Cr_iB_s is a much less effective recombination center than previously assumed. The hole capture cross section of the Cr_iB_s pair of $\sigma_p=1\times10^{-14}$ cm^2 extracted from our combined DLTS and lifetime measurements is in excellent agreement with the value of $\sigma_p=2\times10^{-14}$ cm^2 measured by Hangleiter[16] at 300 K. However, it is well below the value of $\sigma_p=8\times10^{-14}$ cm^2 determined by Dubois *et al.*[10] In the lifetime analysis of Dubois *et al.*, the very large electron capture cross section determined by Mishra has been used to extract σ_p, which makes the σ_p value determined by Hangleiter the more reliable one.

C. Impact of doping concentration

Inconsistent results have been published in the literature concerning the recombination activity of Cr_iB_s pairs in comparison with that of isolated Cr_i. While some authors[9,42] reported that Cr_iB_s pairs are stronger recombination centers than Cr_i, this behavior was not observed by others.[43] Our results suggest that this discrepancy might be attributed to the different base doping concentrations of the *p*-type silicon wafers used in different studies. While Horanyi *et al.*,[42] for example, measured silicon wafers with a boron doping concentration of $\sim10^{15}$ cm^{-3}, Park and Schroder[43] used wafers of much higher doping concentrations around 10^{16} cm^{-3}. In fact, it turns out that the defect parameters for Cr_i and Cr_iB_s pairs determined in the present study imply that the recombination activity of the two centers depends crucially on the

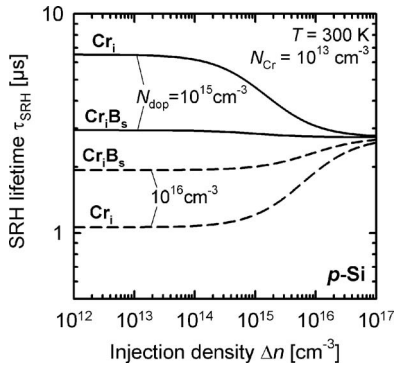

FIG. 10. Calculated injection-dependent SRH lifetime $\tau_{SRH}(\Delta n)$ in p-type silicon of two different doping concentrations N_{dop} with a total chromium contamination level of $N_{Cr}=1\times10^{13}$ cm^{-3}. The defect parameters of Cr_i and Cr_iB_s determined in this study are used. Complete association and dissociation of the Cr_iB_s pairs is assumed, respectively.

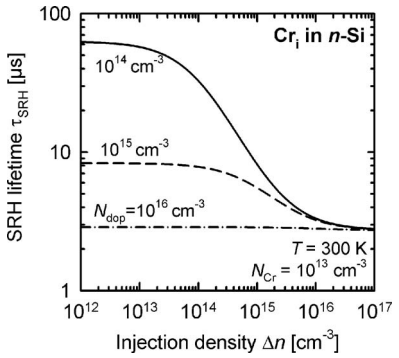

FIG. 11. Calculated injection-dependent SRH lifetime $\tau_{SRH}(\Delta n)$ in n-type silicon of three different doping concentrations N_{dop} with a chromium concentration of $N_{Cr}=1\times10^{13}$ cm^{-3}.

doping concentration N_{dop} of the p-Si material. Figure 10 shows the SRH lifetime calculated for a total chromium concentration of $N_{Cr}=1\times10^{13}$ cm^{-3} using Eq. (1) in combination with the defect parameters of Cr_i and Cr_iB_s determined in this work and assuming complete association and complete dissociation of the Cr_iB_s pairs, respectively. At low injection levels the SRH lifetime saturates for both Cr-related centers, at high injection levels all lifetimes converge to a single value. In lightly doped p-Si with $N_{dop}=1\times10^{15}$ cm^{-3}, the Cr_iB_s pairs give a low-injection lifetime of only 3 µs, whereas isolated Cr_i gives 6.5 µs and is, hence, about two times less recombination active than the Cr_iB_s center. The situation is reversed at the higher doping concentration of $N_{dop}=10^{16}$ cm^{-3}, where Cr_i is the two times stronger recombination center, resulting in a low-injection lifetime of only 1 µs. For $N_{dop}=4\times10^{15}$ cm^{-3} the two Cr-related centers produce identical SRH lifetimes (not shown in Fig. 10), meaning that at this particular doping level both centers show the same recombination activity in p-type silicon. This analysis clearly demonstrates that the doping concentration plays a crucial role in the assessment of the recombination activity of Cr_i versus Cr_iB_s pairs in p-type silicon. Note that for Cr_i the doping dependence of the low-injection SRH lifetime in p-Si is given by the simple expression $\tau_{SRH.li}=\tau_{n0}+\tau_{p0}n_1/N_{dop}$, which is a special case of Eq. (1) for a defect level being located in the upper half of the silicon band gap.

Figure 11 shows the influence of N_{dop} on the SRH lifetime of n-type silicon with a Cr_i concentration of 1×10^{13} cm^{-3}, calculated using the recombination parameters of interstitial chromium determined in this work. As derived directly from Eq. (1), the high-injection SRH lifetime is given by $\tau_{SRH.hi}=\tau_{n0}+\tau_{p0}$ and is therefore, as in the p-type material, independent of N_{dop}. In n-Si with a defect level in the upper half of the silicon band gap, such as Cr_i, the low-injection SRH lifetime can be expressed as $\tau_{SRH.li}=\tau_{p0}(1+n_1/N_{dop})$. Using Eq. (3) with the energy level of Cr_i in Si of $E_C-E_t=0.24$ eV, we calculate $n_1=2\times10^{15}$ cm^{-3}, implying that $\tau_{SRH.li}$ increases strongly with decreasing N_{dop} for doping levels below $\sim4\times10^{15}$ cm^{-3}. As a consequence, the low-injection lifetime in Fig. 11 increases from 3 µs at a doping level of 10^{16} cm^{-3} to 60 µs at 10^{14} cm^{-3}. Hence, in p-Si as well as in n-Si the recombination activity of Cr_i can be strongly reduced by decreasing the doping concentration, whereas the recombination activity of Cr_iB_s pairs in p-Si shows only a weak dependence on N_{dop} in the device-relevant doping range between 10^{15} and 10^{16} cm^{-3} (see Fig. 10).

D. Determination of chromium concentrations in *p*-type silicon

Due to the observed changes in the carrier lifetime before and after dissociation of the Cr_iB_s pairs in p-type silicon, it is possible to determine the chromium concentration in p-Si directly from lifetime measurements. This method was originally developed for the determination of iron concentrations in boron-doped silicon,[44–46] but can in principle be applied to all impurities interacting with the dopant atoms and thereby changing the carrier lifetime of the sample. Assuming τ_a is the measured lifetime before dissociation and τ_d is the lifetime after complete dissociation of all Cr_iB_s pairs, which can, e.g., be realized by a 30-min anneal at 250 °C, the interstitial chromium concentration in the wafer can be expressed as[10]

$$[Cr_i]=C(\Delta n,N_{dop})\left(\frac{1}{\tau_d}-\frac{1}{\tau_a}\right), \tag{7}$$

where the calibration factor C is a function of the injection density Δn and the doping concentration N_{dop} and can be calculated by means of Eq. (1) using the defect parameters determined earlier. Figure 12 shows the calculated inverse calibration factor $1/C$ as a function of injection level Δn for different doping concentrations N_{dop}. At low doping concentrations $N_{dop}<4\times10^{15}$ cm^{-3}, C is negative due to the fact that the Cr_iB_s pair is more recombination active than Cr_i and, hence, $\tau_a<\tau_d$. For higher doping levels $N_{dop}>4\times10^{15}$ cm^{-3}, C is positive and decreases strongly with increasing doping concentration N_{dop}. For $N_{dop}=4\times10^{15}$ cm^{-3}, the method fails as no change in the lifetime can be measured and, hence, $\tau_a=\tau_d$. In the important special case of low injection levels $\Delta n\ll N_{dop}$, the calibration constant approaches a saturation value, which only depends on N_{dop}. Using Eq. (1) with the corresponding Cr_i and Cr_iB_s defect parameters, the inverse low-injection calibration constant $1/C_{li}$ can be expressed as

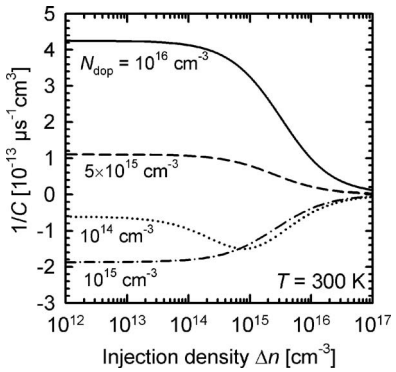

FIG. 12. Inverse calibration factor $1/C$ for the determination of the Cr_i concentration in B-doped p-type silicon, as a function of injection density Δn and doping concentration N_{dop}.

$$\frac{1}{C_{li}(N_{dop})} = \frac{v_{th}}{\frac{1}{\sigma_n^{Cr_i}} + \frac{1}{\sigma_p^{Cr_i}}\frac{n_1^{Cr_i}}{N_{dop}}} - \frac{v_{th}}{\frac{1}{\sigma_n^{CrB}}\left(1 + \frac{p_1^{CrB}}{N_{dop}}\right)}, \tag{8}$$

where $n_1^{Cr_i}=2\times10^{15}$ cm^{-3}, $p_1^{CrB}=4\times10^{14}$ cm^{-3}, $\sigma_n^{Cr_i}=2\times10^{-14}$ cm^2, $\sigma_p^{Cr_i}=4\times10^{-15}$ cm^2, and $\sigma_n^{CrB}=5\times10^{-15}$ cm^2. For $N_{dop}>4\times10^{15}$ cm^{-3}, p_1^{CrB}/N_{dop} can be neglected and Eq. (8) simplifies to

$$\frac{1}{C_{li}(N_{dop})} = \left(\frac{N_{dop}}{N_{dop}/\sigma_n^{Cr_i} + n_1^{Cr_i}/\sigma_p^{Cr_i}} - \sigma_n^{CrB}\right)v_{th}. \tag{9}$$

The accuracy of this method for the determination of the interstitial chromium concentration in boron-doped p-type silicon depends on the reliability of the experimentally determined defect parameters entering into Eqs. (8) and (9). Due to the uncertainty ranges of the defect parameters determined in this study, we estimate that the chromium concentration can be determined down to $\sim10^{10}$ cm^{-3} with an accuracy of a factor of 2.

V. CONCLUSIONS

We have determined the recombination parameters of isolated Cr_i and Cr_iB_s pairs in silicon with hitherto unattained accuracy by combining DLTS and TIDLS measurements on deliberately chromium-contaminated phosphorus-doped n- and boron-doped p-type silicon wafers. On the n-type silicon material, it was possible to pin down energy level as well as capture cross sections of the Cr_i donor level to $E_C-E_t=0.24$ eV, $\sigma_n=2\times10^{-14}$ cm^2, and $\sigma_p=4\times10^{-15}$ cm^2. Electron as well as hole capture cross sections were found to be independent of temperature, suggesting that the recombination dominantly occurs via the multiphonon capture mechanism. In the case of Cr_iB_s pairs in p-type silicon, the Arrhenius plot of the Cr_iB_s-related DLTS peak resulted in an energy level of $E_t-E_V=0.28$ eV, which was used in the SRH analysis of the injection-dependent lifetime curve measured at 25 °C to extract the capture cross sections of the Cr_iB_s donor in silicon to $\sigma_n=5\times10^{-15}$ cm^2 and $\sigma_p=1\times10^{-14}$ cm^2. The hole capture cross section was found to be in excellent agreement with the results from the DLTS Arrhenius plot and the filling pulse variation method. No temperature dependence was found for the electron and the hole capture cross sections, suggesting that electron-hole recombination via Cr_iB_s pairs proceeds via multiphonon capturing. Inserting the defect parameters into the SRH equation allowed us to show that it depends strongly on the doping concentration whether Cr_i or Cr_iB_s pairs are the more recombination-active centers, although both defects are amongst the strongest known recombination centers in silicon. The latter statement holds despite the fact that the capture cross sections for Cr_i and Cr_iB_s determined in this study are about one order of magnitude lower than the most frequently used capture cross sections published in the literature.

Lifetime changes before and after thermal dissociation of Cr_iB_s pairs were shown to be usable to extract the Cr_i concentration in boron-doped p-type silicon. The calibration function required to convert the lifetime changes into the Cr_i concentration was calculated using the measured defect parameters. Except of doping concentrations around 4×10^{15} cm^{-3}, where Cr_i and Cr_iB_s pairs show the same recombination activity, the method makes it possible to determine the level of chromium contamination in boron-doped p-type silicon with an extremely high sensitivity of $\sim10^{10}$ cm^{-3}.

ACKNOWLEDGMENTS

The authors thank Rolf Brendel (ISFH) for valuable discussions and Takao Abe (Shin-Etsu Handotai) for providing the chromium-contaminated silicon wafers. This work was funded by the State of Lower Saxony and the German Federal Ministry for the Environment, Nature Conservation, and Nuclear Safety (BMU) under Contract No. 0327650C.

[1] J. R. Davis, A. Rohatgi, R. H. Hopkins, P. D. Blais, P. Rai-Choudhury, J. R. Mccormick, and H. C. Mollenkopf, IEEE Trans. Electron Devices **ED-27**, 677 (1980).
[2] D. Macdonald, A. Cuevas, A. Kinomura, and Y. Nakano, *Proceedings of the 29th IEEE Photovoltaics Specialists Conference*, New Orleans, LA (IEEE, New York, 2002), p. 285.
[3] D. Macdonald, A. Cuevas, A. Kinomura, Y. Nakano, and L. J. Geerligs, J. Appl. Phys. **97**, 033523 (2005).
[4] A. A. Istratov, T. Buonassisi, R. J. McDonald, A. R. Smith, R. Schindler, J. A. Schindler, J. A. Rand, J. P. Kalejs, and E. R. Weber, J. Appl. Phys. **94**, 6552 (2003).
[5] T. Buonassisi, A. A. Istratov, M. D. Pickett, M. Heuer, J. P. Kalejs, G. Hahn, M. A. Marcus, B. Lai, Z. Cai, S. M. Heald, T. F. Ciszek, R. F. Clark, D. W. Cunningham, A. M. Gabor, R. Jonczyk, S. Narayanan, E. Sauar, and E. R. Weber, Prog. Photovolt. Res. Appl. **14**, 513 (2006).
[6] H. H. Woodbury and G. W. Ludwig, Phys. Rev. **117**, 102 (1960).
[7] G. W. Ludwig and H. H. Woodbury, Solid State Phys. **13**, 223 (1962).
[8] E. R. Weber, Appl. Phys. A: Solids Surf. **30**, 1 (1983).
[9] K. Mishra, Appl. Phys. Lett. **68**, 3281 (1996).
[10] S. Dubois, O. Palais, and P. J. Ribeyron, Appl. Phys. Lett. **89**, 232112 (2006).
[11] K. Graff, *Metal Impurities in Silicon-Device Fabrication*, 2nd ed. (Springer, Berlin, 2000).
[12] K. Graff and H. Pieper, *Semiconductor Silicon 1981* (The Electrochemical Society, Pennington, NJ, 1981), p. 331.
[13] H. Conzelmann, K. Graff, and E. R. Weber, Appl. Phys. A: Solids Surf. **30**, 169 (1983).
[14] H. Feichtinger and R. Czaputa, Appl. Phys. Lett. **39**, 706 (1981).
[15] N. Achtziger, T. Licht, U. Reislöhner, M. Rüb, and W. Witthuhn, *The Physics of Semiconductors* (World Scientific, Singapore, 1996), p. 2717.
[16] A. Hangleiter, Phys. Rev. B **35**, 9149 (1987).
[17] S. Dubois, O. Palais, and P. J. Ribeyron, Appl. Phys. Lett. **89**, 232112 (2006).

[18]F. Shimura, T. Okui, and T. Kusama, J. Appl. Phys. **67**, 7168 (1990).
[19]J. Schmidt and K. Bothe, Phys. Rev. B **69**, 024107 (2004).
[20]T. Lauinger, J. Schmidt, A. G. Aberle, and R. Hezel, Appl. Phys. Lett. **68**, 1232 (1996).
[21]J. Schmidt and A. G. Aberle, J. Appl. Phys. **81**, 6186 (1997).
[22]R. A. Sinton and A. Cuevas, Appl. Phys. Lett. **69**, 2510 (1996).
[23]J. Schmidt, Appl. Phys. Lett. **82**, 2178 (2003).
[24]J. Schmidt and R. Sinton, Proceedings of the 3rd World Conference on Photovoltaic Energy Conversion, Osaka, Japan, 2003, p. 947 (unpublished).
[25]N. D. Arora, J. R. Hauser, and D. J. Roulston, IEEE Trans. Electron Devices **29**, 292 (1982).
[26]D. Macdonald and A. Cuevas, Phys. Rev. B **67**, 075203 (2003).
[27]W. Shockley and W. T. Read, Phys. Rev. **87**, 835 (1952).
[28]R. N. Hall, Phys. Rev. **87**, 387 (1952).
[29]J. S. Blakemore, *Semiconductor Statistics* (Dover, Mineola, NY, 1987).
[30]W. M. Bullis and H. R. Huff, J. Electrochem. Soc. **143**, 1399 (1996).
[31]M. A. Green, J. Appl. Phys. **67**, 2944 (1990).
[32]S. Weiss and R. Kassing, Solid-State Electron. **31**, 1733 (1988).
[33]S. Weiss, R. Beckmann, and R. Kassing, Appl. Phys. A: Solids Surf. **50**, 151 (1990).
[34]S. Rein, S. Diez, and S. W. Glunz, *Proceedings of the 19th European Photovoltaic Solar Energy Conference*, Paris, France (WIP, Munich, 2004), p. 219.
[35]S. Rein, *Lifetime Spectroscopy*, Springer Series in Materials Science Vol. 85 (Springer, Heidelberg, 2005).
[36]V. N. Abakumov, V. I. Perel, and I. N. Yassievich, *Nonradiative Recombination in Semiconductors* (North-Holland, Amsterdam, 1991).
[37]J. H. Reiss, R. R. King, and F. J. Morin, Bell Syst. Tech. J. **35**, 535 (1956).
[38]H. Nakashima, T. Sadoh, H. Kitagawa, and K. Hashimoto, Mater. Sci. Forum **143–147**, 761 (1994).
[39]D. Macdonald, T. Roth, P. Deenapanray, K. Bothe, P. Pohl, and J. Schmidt, J. Appl. Phys. **98**, 083509 (2005).
[40]L. C. Kimerling and J. L. Benton, Physica B (Amsterdam) **116B**, 297 (1983).
[41]J. Criado, A. Gomez, E. Calleja, and E. Munoz, Appl. Phys. Lett. **52**, 660 (1988).
[42]T. S. Horanyi, P. Tütto, and C. Kovacsics, J. Electrochem. Soc. **143**, 216 (1996).
[43]S. H. Park and D. K. Schroder, J. Appl. Phys. **78**, 801 (1995).
[44]M. Kittler, W. Seifert, K. Schmalz, and K. Tittelbach-Helmrich, Phys. Status Solidi A **96**, K133 (1986).
[45]G. Zoth and W. Bergholz, J. Appl. Phys. **67**, 6764 (1990).
[46]J. Schmidt and D. Macdonald, J. Appl. Phys. **97**, 113712 (2005).